INTERNATIONAL JOURNAL FOR NUMERICAL METHODS IN FLUIDS, VOL. 11, 969–984 (1990)

OPEN BOUNDARY CONDITION SYMPOSIUM BENCHMARK SOLUTION: STRATIFIED FLOW OVER A BACKWARD-FACING STEP

JOHN M. LEONE JR.

Lawrence Livermore National Laboratory, P.O. Box 808, L-262, Livermore, CA 94550, U.S.A.

SUMMARY

This paper presents a detailed numerical solution to a simplified version of two-dimensional stratified flow over a backward-facing step with a Froude number of 16/9, a Reynolds number of 800 and a Prandtl number of 1—one of the Open Boundary Condition Symposium test problems. The steady state solution was derived by integrating the time-dependent Boussinesq equations forward in time using a semi-implicit finite-element-based model on a 38400-element mesh. In addition to presenting the results derived on this grid, the paper also presents the results of a Richardson extrapolation calculation for a set of 'key' parameters. It is hoped that this solution can be used as a baseline to compare the performance of the various techniques discussed at the Open Boundary Condition Symposium.

KEY WORDS Finite element Boussinesq Open boundary conditions Stratified backward-facing step

1. INTRODUCTION

The Open Boundary Condition Symposium was conceived as a forum to exchange ideas and techniques for approximating 'open boundaries'. Open boundaries are computational boundaries that are most often artificial in the sense that while the simulation is supposed to represent flow in a very large or even infinite domain, the computational domain is truncated due to computational limitations, thus imposing an artificial outflow boundary on the problem. The stratified flow over a backward-facing step is one of a set of trial problems proposed to provide a common test bed for the discussions. The purpose of this paper is to present an accurate and detailed solution to the problem. These data can then be used to measure the performance of prospective open boundary conditions.

2. THE PROBLEM

The problem is a simplified version of stratified flow over a backward-facing step in an infinite domain. The problem domain and specified boundary conditions are shown in Figure 1. (Note that the step has been approximated by a parabolic inflow over a no-slip insulated wall for computational convenience.)

0271-2091/90/150969–16$08.00

Received 21 March 1990
Revised 7 May 1990

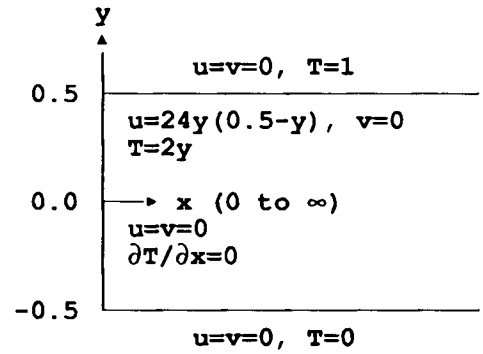

Figure 1. Continuum problem

The equations used in the simulation were the 2D non-dimensional Boussinesq equations

$$\frac{\partial \mathbf{u}}{\partial t} + \mathbf{u}\cdot\nabla\mathbf{u} = -\nabla P + Re^{-1}\nabla^2\mathbf{u} + Fr^{-1}\mathbf{k}T, \tag{1}$$

$$\nabla\cdot\mathbf{u} = 0, \tag{2}$$

$$\frac{\partial T}{\partial t} + \mathbf{u}\cdot\nabla T = Pe^{-1}\nabla^2 T, \tag{3}$$

where $\mathbf{k}$ is the unit vector in the y-direction, $Re \equiv u_0 H/\nu$ is the Reynolds number, $Fr \equiv (u_0/u_B)^2$ is the Froude number and $Pe \equiv PrRe$ is the Peclet number, with $Pr \equiv \nu/\kappa$ the Prandtl number. Here u_0 is the average inlet velocity, H is the height of the channel, H/u_0 is the characteristic time and $u_B = NH$ is the buoyancy velocity, with $N = (\gamma g \Delta T/H)^{1/2}$ the Brunt–Vaisala frequency; γ is the volumetric expansion coefficient and g is 'gravity'.

The parameters chosen for the simulation reported here were $Pr = 1$, $Fr = 16/9$ and $Re = Pe = 800$. Defining the Richardson number as $Ri = 1/Fr$, the Grashof number as $Gr = Re^2/Fr$ and the Rayleigh number as $Ra = PrGr$ yields $Ri = 9/16$ and $Gr = Ra = 3.6 \times 10^5$.

3. THE SOLUTION METHOD

The method used solves the time-dependent Boussinesq equations of motion and temperature. The spatial discretization used the finite element method employing bilinear finite elements for temperature and velocity, piecewise constant elements for pressure, and lumped mass in the time derivatives. The time integration scheme was the semi-implicit backward Euler scheme of Gresho and Chan[1] wherein the advection terms are integrated via forward Euler with balancing tensor diffusivity (BTD) and the diffusion terms are integrated via backward Euler. In order to stabilize the scheme with respect to gravity (buoyancy) waves, the forward–backward scheme of Sun[2] is used wherein the temperature is first advanced in time to $n+1$, then the temperature at $n+1$ is used in the buoyancy term of the pressure and momentum equations. In more detail: first the temperature is updated via

$$(\mathbf{I} + \Delta t \mathbf{M}_s^{-1}\mathbf{K}_{s_n})\mathbf{T}_{n+1} = \mathbf{T}_n + \Delta t \mathbf{M}_s^{-1}[\mathbf{F}_n^T - \mathbf{N}_s(\mathbf{u}_n)\mathbf{T}_n]; \tag{4}$$

next the pressure is calculated from the 'consistent' Poisson equation using $\mathbf{T}_{n+1}$ in the buoyancy term via

$$(\mathbf{C}^{\mathrm{T}}\mathbf{M}^{-1}\mathbf{C})\mathbf{P}_n = \mathbf{C}^{\mathrm{T}}\left(\mathbf{M}^{-1}[\mathbf{F}_n - \mathbf{N}(\mathbf{u}_n)\mathbf{u}_n - \mathbf{K}_n\mathbf{u}_n] + \frac{\mathbf{u}_n}{\Delta t}\right); \tag{5}$$

and finally the velocity is updated via

$$(\mathbf{I} + \Delta t\mathbf{M}^{-1}\mathbf{K}_n)\mathbf{u}_{n+1} = \mathbf{u}_n + \Delta t\mathbf{M}^{-1}[\mathbf{F}_n - \mathbf{N}(\mathbf{u}_n)\mathbf{u}_n - \mathbf{C}\mathbf{P}_n]. \tag{6}$$

In the above equations, $\mathbf{T}$ is a vector of length n (the number of node points) of nodal temperature values, $\mathbf{u}$ is a vector of length $2n$ containing both nodal velocity components, and $\mathbf{P}$ is a vector of length m (the number of elements) containing the element pressures. $\mathbf{M}$ is the $2n \times 2n$ lumped mass matrix, $\mathbf{K}$ is the $2n \times 2n$ diffusion plus BTD matrix, $\mathbf{N}$ is the $2n \times 2n$ non-linear advection matrix, $\mathbf{C}$ is the $2n \times m$ gradient matrix and its transpose is the $m \times 2n$ divergence matrix. The subscript 's' indicates similar matrices of size $n \times n$. $\mathbf{F}$ is a vector of length $2n$ containing boundary conditions and the buoyancy terms for the momentum equation and is thus a function of $\mathbf{T}_{n+1}$, while $\mathbf{F}^{\mathrm{T}}$ is the vector of length n containing boundary conditions and source terms for the temperature. $\mathbf{N}$, $\mathbf{C}$ and the BTD matrix are approximated via one-point Gaussian quadrature. All other matrices are evaluated with full Gaussian quadrature.

The Poisson equation was solved via a direct skyline solver, while the linear systems for the velocity components and the temperature were solved using a diagonally scaled conjugate gradient method.

4. THE SIMULATION

The computational domain and boundary conditions used in the simulation are shown in Figure 2. The outflow was taken to be a distance of 30 units downstream from the inlet, i.e. twice the length of the longer test domain. The outflow boundary conditions used were based on the finite element 'natural boundary conditions', which here are

$$f_{\mathrm{n}} = -P + Re^{-1}\frac{\partial u}{\partial x} \quad \text{and} \quad f_{\mathrm{t}} = Re^{-1}\frac{\partial v}{\partial x}, \tag{7}$$

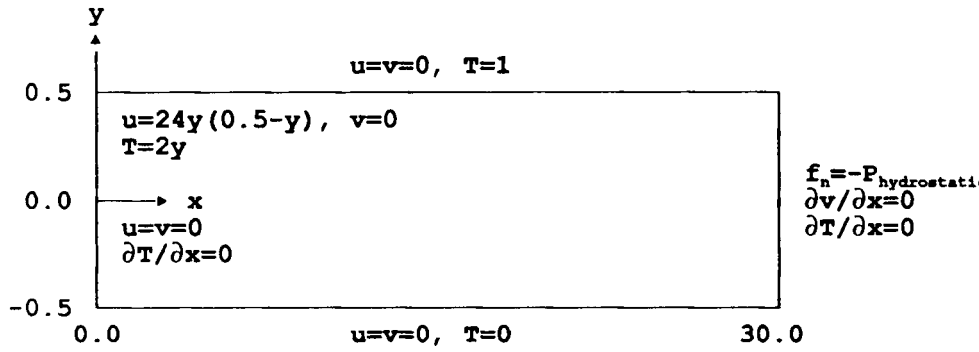

Figure 2. Computational domain and boundary conditions

where f_n and f_t are the specified pseudo-tractions. We used $f_t = 0$ and $f_n = -P_{\text{hydrostatic}}$ à la Leone *et al.*,[3] i.e.

$$f_n(y, t) \simeq Fr^{-1} \int_y^{0.5} T(30, y', t)\, dy'. \tag{8}$$

The outflow boundary condition for T is also the natural boundary condition $\partial T/\partial x = 0$.

On the basis of preliminary calculations on coarser grids, a final grid of 80 × 480 equal-size rectangular elements for a total of 38400 elements, 38961 nodes and 155283 unknowns was selected. The resulting element sizes were $\Delta x = 0{\cdot}0625$ by $\Delta y = 0{\cdot}0125$. The simulation was integrated forward in time from an initial state that corresponds to a potential flow of an isothermal ($T = 0$) fluid forced with the inflow boundary conditions. The integration continued to $t = 400$ time units. Analysis of plots of the time history curves for the unknowns at several nodes as well as comparisons of global field plots indicate that steady state was achieved at approximately 200 time units.

Figure 3 shows a comparison of the calculated u-velocity, temperature and vorticity profiles at the domain outlet boundary $x = 30$ with the analytic stratified Poiseuille flow solution that would obtain far from the step. It shows that the u-velocity is within 1% of the asymptotic analytic solution, the temperature profile is within 1·25% and the vorticity is within 2%. This is a strong indication that the outflow boundary is 'far enough' away from the step and the boundary conditions were well enough behaved that the solution is not significantly perturbed by the finite domain.

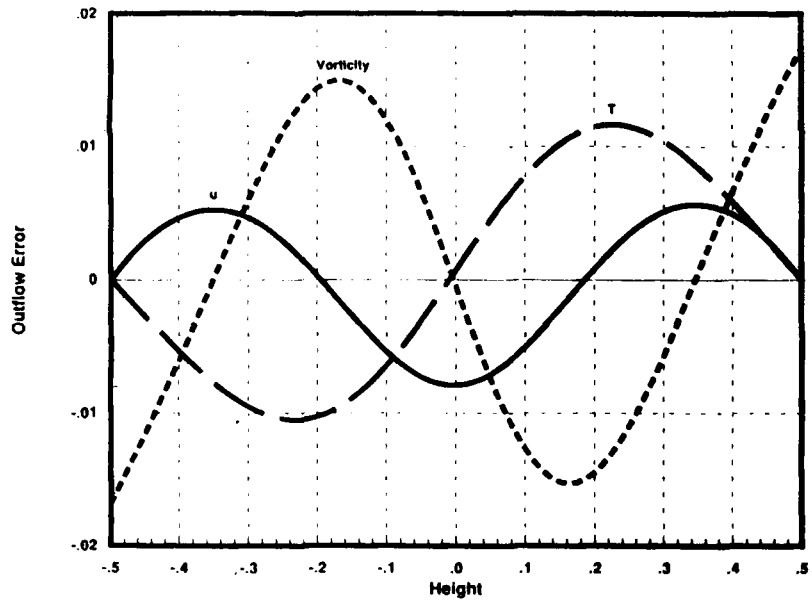

Figure 3. Vertical profiles at the domain boundary $x = 30$ of the normalized difference between the calculated value and the analytic stratified Poiseuille flow solution of the u-component of velocity (solid line), the temperature (dashed line) and the vorticity (dotted line)

5. RESULTS

The steady state flow configuration for the test problem long domain, $0 \leqslant x \leqslant 15$, is illustrated in Figures 4 and 5. The core of the flow descends from the inlet, rebounds and descends slightly again before filling the channel and approaching the stratified Poiseuille flow solution. There are three eddies on the bottom wall. The first is a very weak counterclockwise-rotating eddy (eddy 1) in the bottom corner of the step. The second (eddy 2) is above and to the right of eddy 1 and is a clockwise-rotating eddy. The third (eddy 3) is also a clockwise-rotating eddy below the main flow at $x \simeq 6$. In addition, there are two counterclockwise-rotating eddies on the top wall, one (eddy 4) located above the main flow near $x \simeq 3$ and the second (eddy 5) located at $x \simeq 9$.

Table I lists the positions and sizes of the five eddies. For the purposes of this benchmark an eddy was said to start at the point where the vorticity on the appropriate wall went through zero and to end at the next wall position with zero vorticity. (For steady two-dimensional flow this

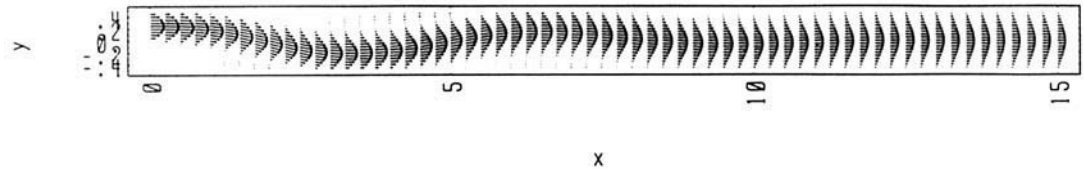

Figure 4. Steady state velocity field on the domain $0 \leqslant x \leqslant 15$. For clarity only every fourth vector is plotted

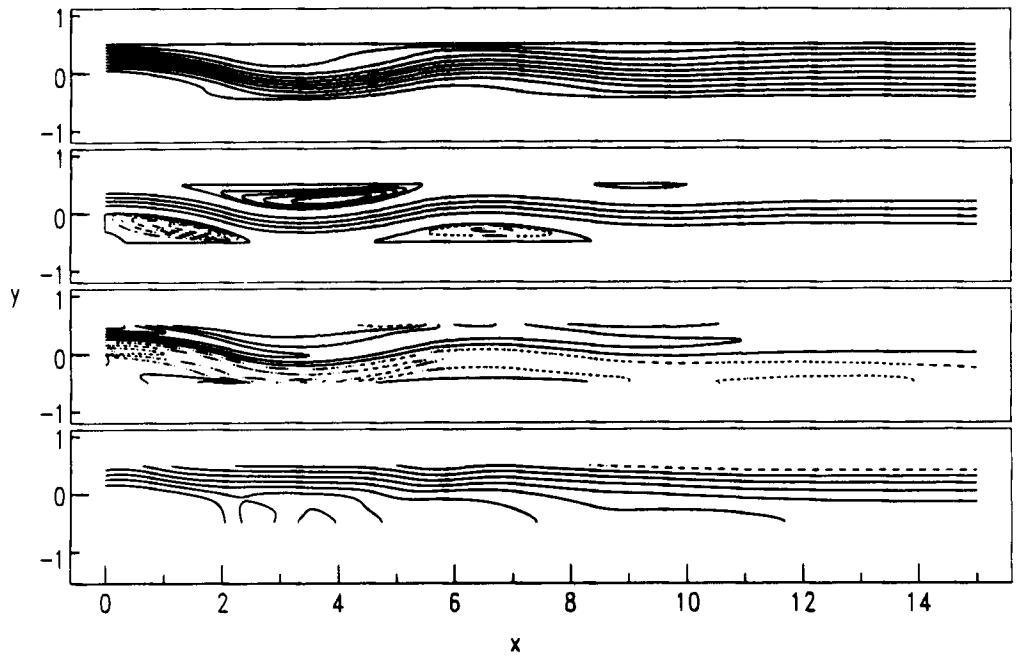

Figure 5. Steady state contours (for streamfunction and vorticity, positive contours solid lines and negative contours dashed lines) of (a) temperature with contour interval of 0·1, (b) streamfunction with contour interval of 0·0994 in the main flow (between the separation streamlines) and 0·004 within the eddies, (c) vorticity with contour interval of 2·3268, and (d) pressure with contour interval of 0·04841 on the domain $0 \leqslant x \leqslant 15$

Table I. Eddy positions and lengths from the 80 × 480 simulation

Eddy	Start x	Stop x	Length
1 (bottom)	0·000	0·356	0·356
2 (bottom)	0·356	2·498	2·142
3 (bottom)	4·548	8·391	3·843
4 (top)	1·210	5·492	4·282
5 (top)	8·164	10·215	2·051

Table II. Eddy streamfunction (extremum minus separation) values and locations from the 80 × 480 simulation

Eddy	Extremum value	x-co-ordinate	y-co-ordinate
1 (bottom)	0·00008	0·0125	−0·4000
2 (bottom)	−0·02239	1·500	−0·2625
3 (bottom)	−0·00851	6·625	−0·3000
4 (top)	0·01880	4·000	0·2375
5 (top)	0·00020	9·187	0·4500

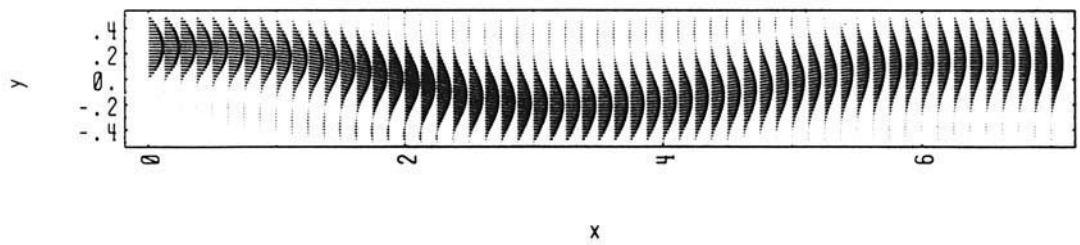

Figure 6. Steady state velocity field on the domain $0 \leqslant x \leqslant 7$. For clarity only every second vector is plotted.

also corresponds to the positions of zero wall shear stress.) The length of the eddy was the distance between the starting and ending positions. This is not truly indicative of the length of eddy 2 of course, but it still provides relevant data for comparison. The strengths of the eddies are indicated by the streamfunction extrema contained within the eddy. These extrema and their positions are listed in Table II. The values reported are the difference between the extremum and the appropriate separation value.

To provide more detail and to facilitate comparisons, the global fields of velocity, temperature, streamfunction, vorticity and pressure are also presented on the second test domain, $0 \leqslant x \leqslant 7$, in Figures 6 and 7. Only eddies 1, 2, and 4 are contained within this truncated domain. Eddy 3 begins within the domain but extends beyond $x = 7$.

The vertical profiles of u, v, T and P at $x = 0$, 3, 7 and 15 are shown in Figures 8–11 respectively. Vertical profiles of streamfunction and vorticity at the same locations are shown in Figures 12 and 13.

For information and comparison, a number of quantities have been calculated at the two test boundaries, $x = 7$ and 15. Those quantities which are spatial derivatives were calculated from the

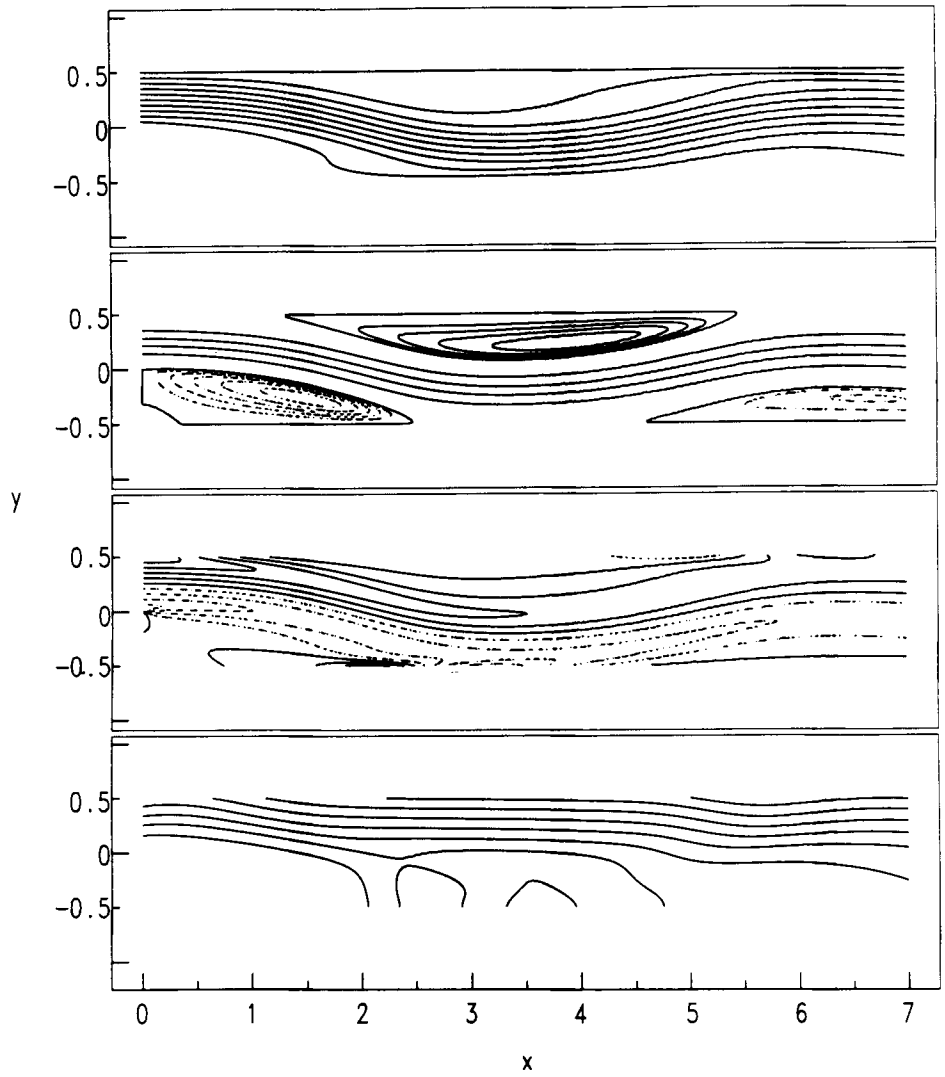

Figure 7. Steady state contours (for streamfunction and vorticity, positive contours solid lines and negative contours dashed lines) of (a) temperature, (b) streamfunction, (c) vorticity and (d) pressure on the domain $0 \leqslant x \leqslant 7$. The contour values plotted are the same as in Figure 5

simulation results using the simplest second-order centred finite difference method. Figures 14–19 present the vertical profiles at $x = 7$ and 15 of $\partial u/\partial x$, $\partial u/\partial y$, $\partial v/\partial x$, $\partial T/\partial x$, $\partial(\text{vorticity})/\partial x$ and $\partial u/\partial y + \partial v/\partial x$ respectively. (Note that the top and bottom wall values of $\partial u/\partial y$ where calculated using appropriate second-order one-sided finite difference approximation.)

In many finite element models the so-called natural boundary condition on a vertical boundary for the u-velocity takes the form of either the normal pseudo-traction

$$f_n = -P + \frac{1}{Re}\frac{\partial u}{\partial x}$$

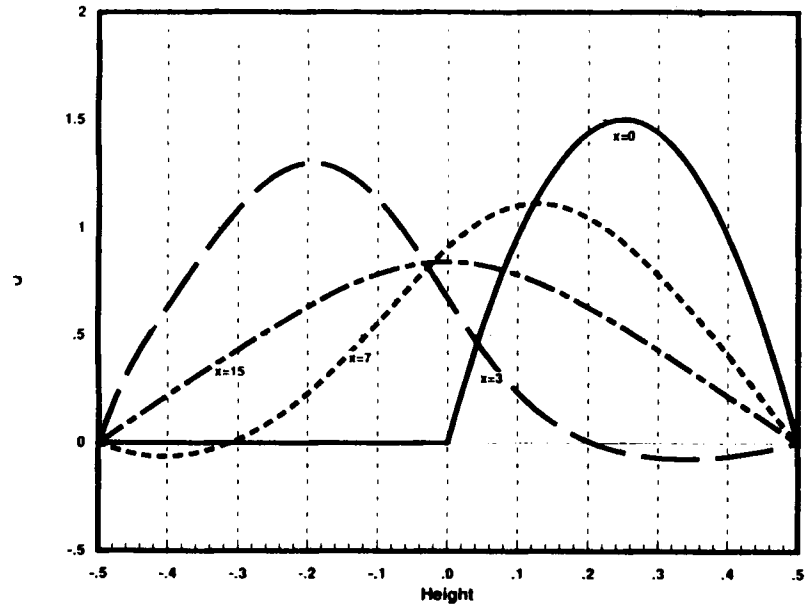

Figure 8. Vertical profiles of the u-velocity at $x = 0$ (solid line), $x = 3$ (dashed line), $x = 7$ (dotted line) and $x = 15$ (chain line)

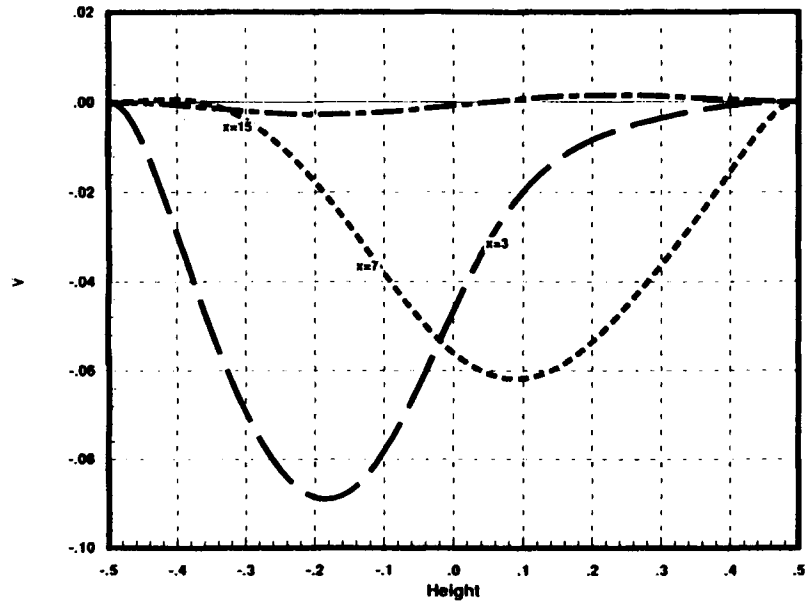

Figure 9. Vertical profiles of the v-velocity at $x = 3$ (dashed line), $x = 7$ (dotted line) and $x = 15$ (chain line)

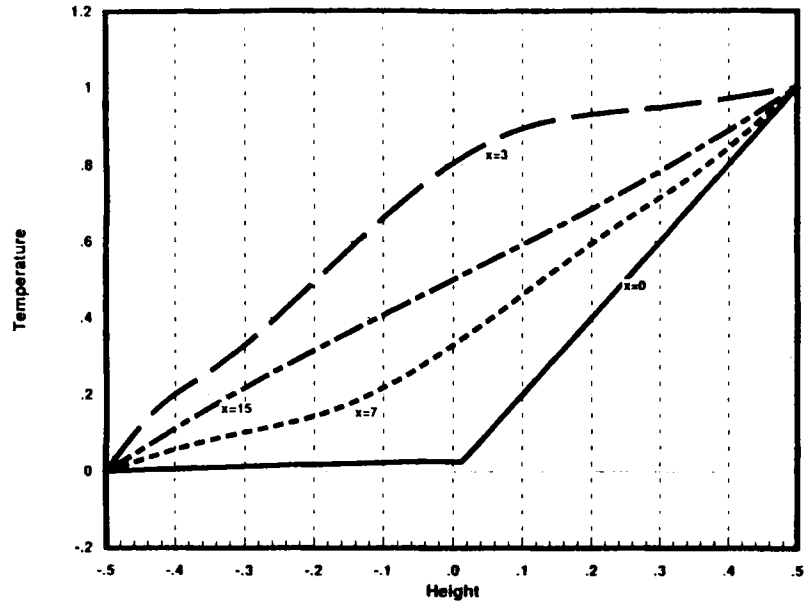

Figure 10. Vertical profiles of the temperature at $x = 0$ (solid line), $x = 3$ (dashed line), $x = 7$ (dotted line) and $x = 15$ (chain line)

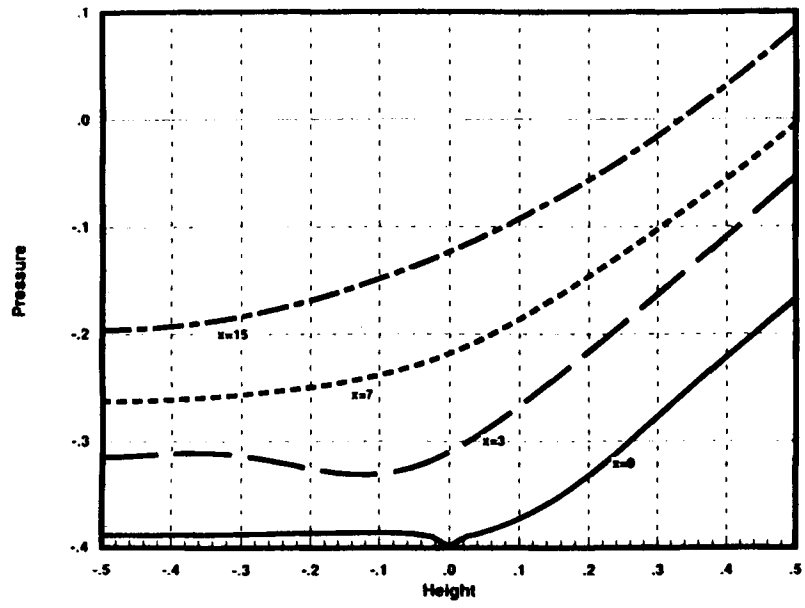

Figure 11. Vertical profiles of the pressure at $x = 0$ (solid line), $x = 3$ (dashed line), $x = 7$ (dotted line) and $x = 15$ (chain line). Note that the pressure field is determined only up to an additive constant, here approximately zero at $x = 30$ and $y = 0{\cdot}5$

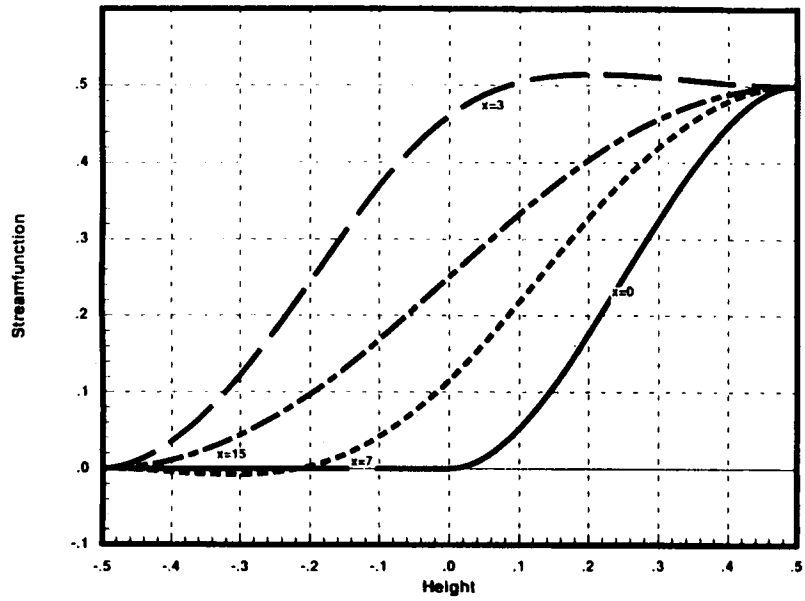

Figure 12. Vertical profiles of the streamfunction at $x = 0$ (solid line), $x = 3$ (dashed line), $x = 7$ (dotted line) and $x = 15$ (chain line)

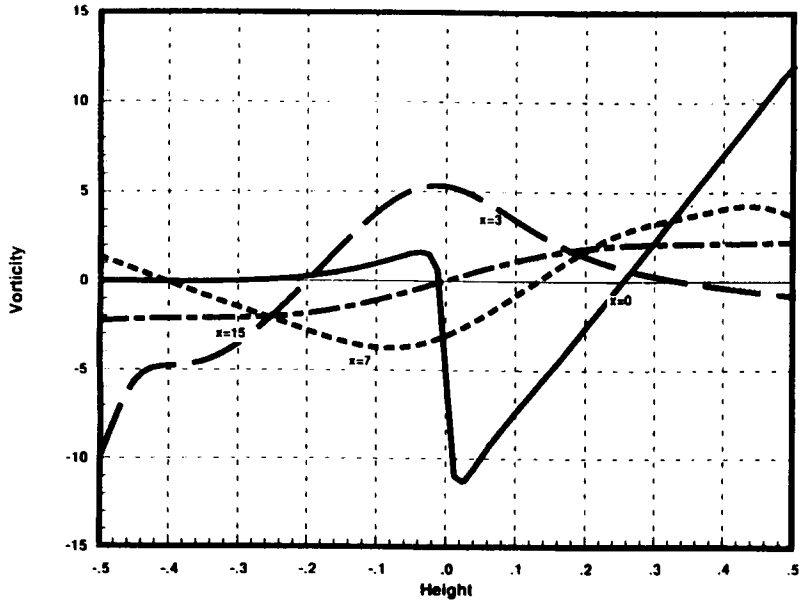

Figure 13. Vertical profiles of the vorticity at $x = 0$ (solid line), $x = 3$ (dashed line), $x = 7$ (dotted line) and $x = 15$ (chain line)

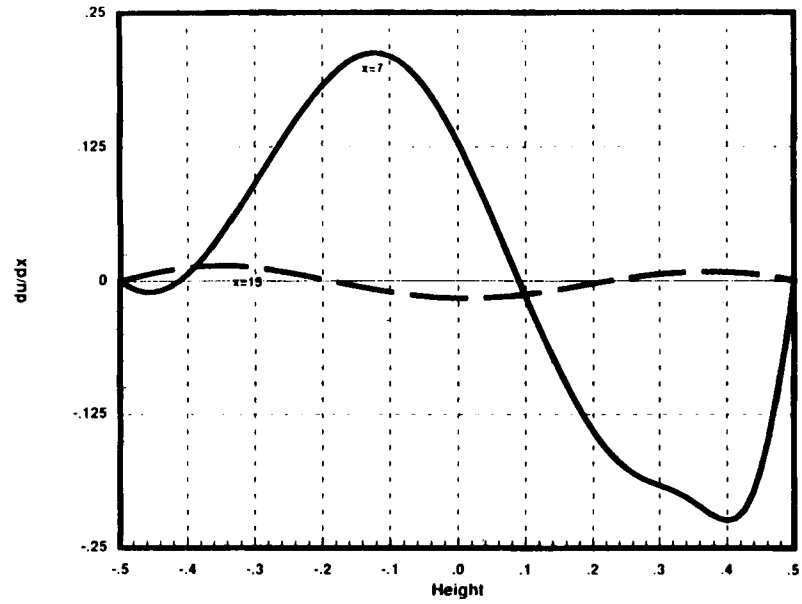

Figure 14. Vertical profiles of $\partial u/\partial x$ at $x = 7$ (solid line) and $x = 15$ (dashed line)

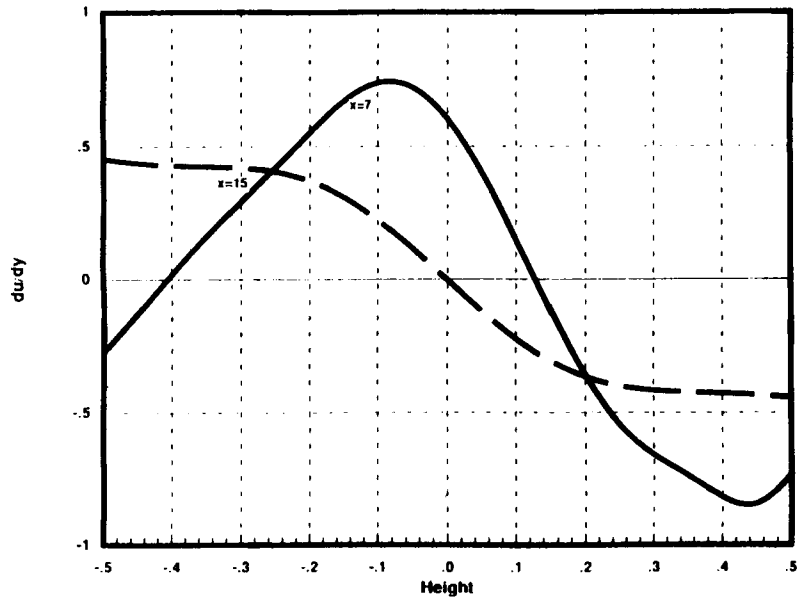

Figure 15. Vertical profiles of $\partial u/\partial y$ at $x = 7$ (solid line) and $x = 15$ (dashed line)

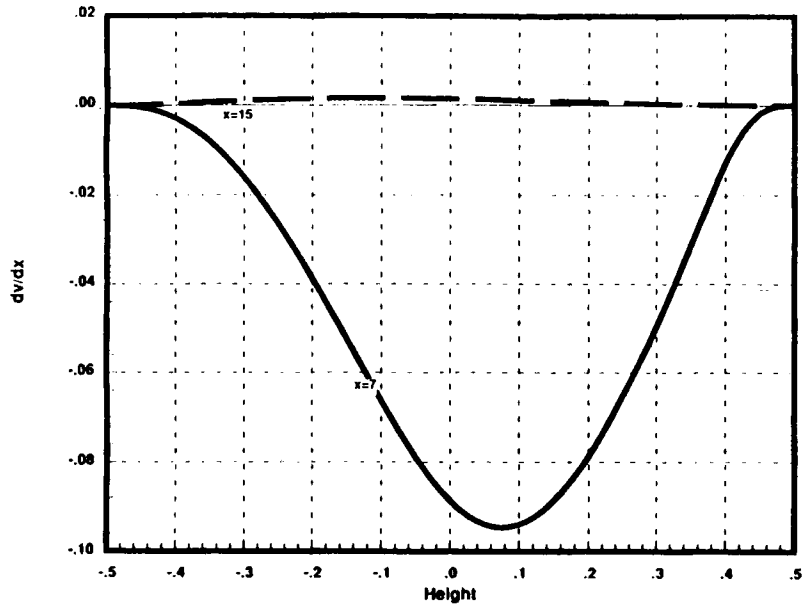

Figure 16. Vertical profiles of $\partial v/\partial x$ at $x = 7$ (solid line) and $x = 15$ (dashed line)

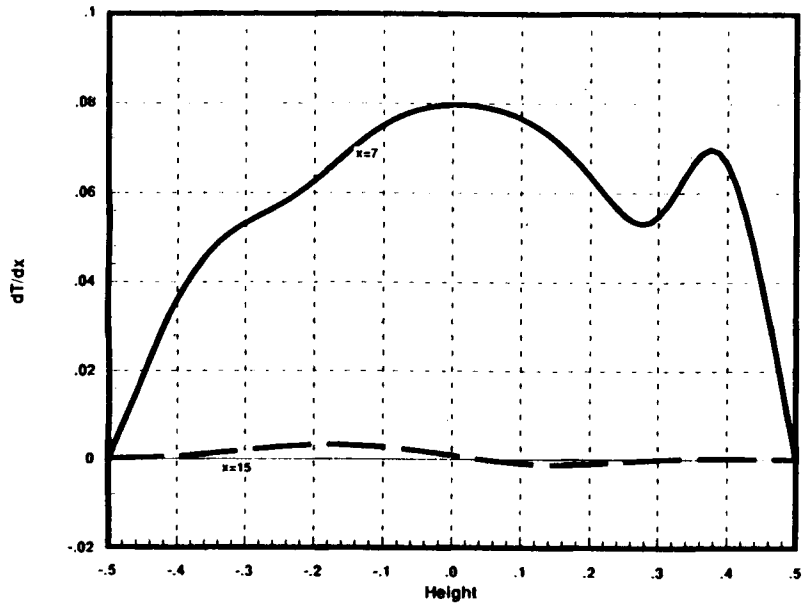

Figure 17. Vertical profiles of $\partial T/\partial x$ at $x = 7$ (solid line) and $x = 15$ (dashed line)

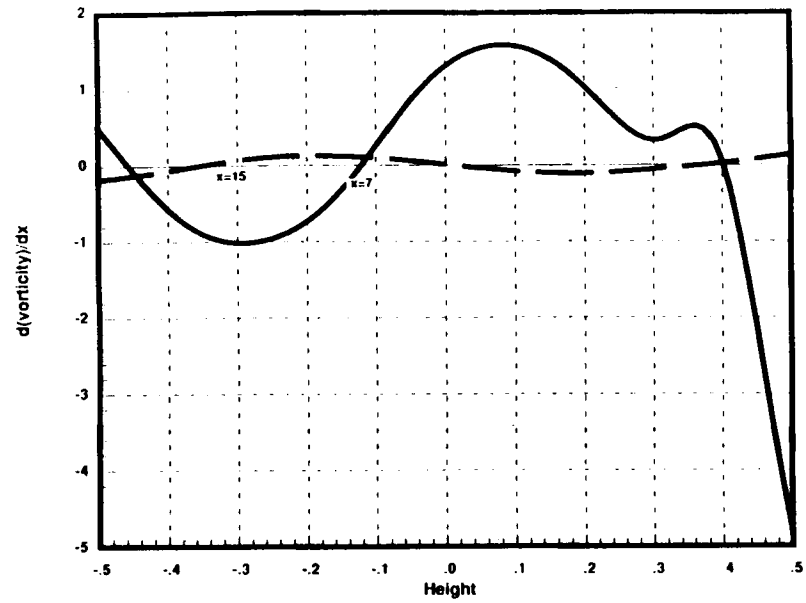

Figure 18. Vertical profiles of $\partial(\text{vorticity})/\partial x$ at $x = 7$ (solid line) and $x = 15$ (dashed line)

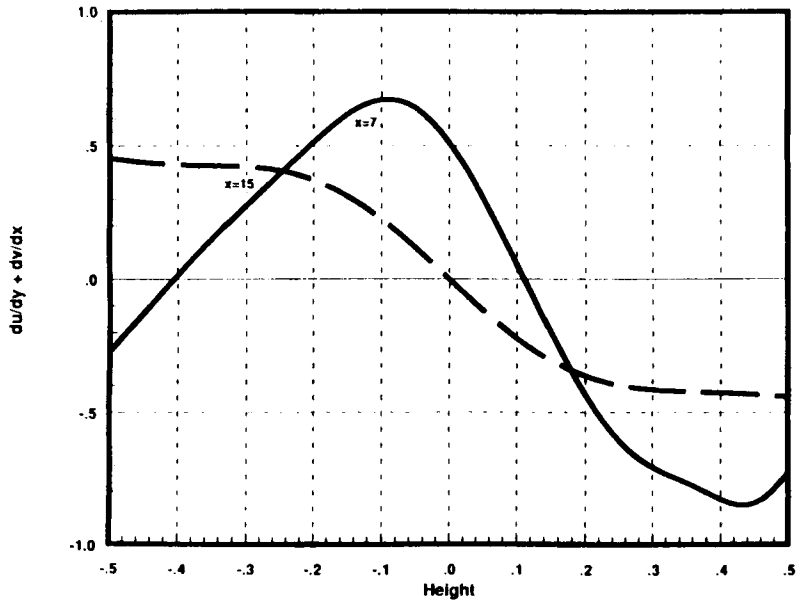

Figure 19. Vertical profiles of $\partial u/\partial y + \partial v/\partial x$ at $x = 7$ (solid line) and $x = 15$ (dashed line)

or the normal traction

$$f_n = -P + \frac{2}{Re}\frac{\partial u}{\partial x},$$

while for v it is either the shear pseudo-traction

$$f_t = \frac{1}{Re}\frac{\partial v}{\partial x}$$

or the shear traction

$$f_t = \frac{1}{Re}\left(\frac{\partial u}{\partial y} + \frac{\partial v}{\partial x}\right).$$

The profiles of the normal pseudo-traction are presented in Figure 20 at $x = 7$ and 15. It is noteworthy that in this case the hydrostatic pressure field is more than three orders of magnitude greater than the normal viscous stress. Thus $f_n = -P$ is a very good approximation for either case.

Given that $-P$ is a good approximation for f_n, the question becomes how to estimate P. One possible method of doing this is to assume that the pressure at the outlet is hydrostatic, i.e. P is a function of y only and can be calculated from the temperature field via

$$\frac{\partial P}{\partial y} = Fr^{-1}T. \tag{9}$$

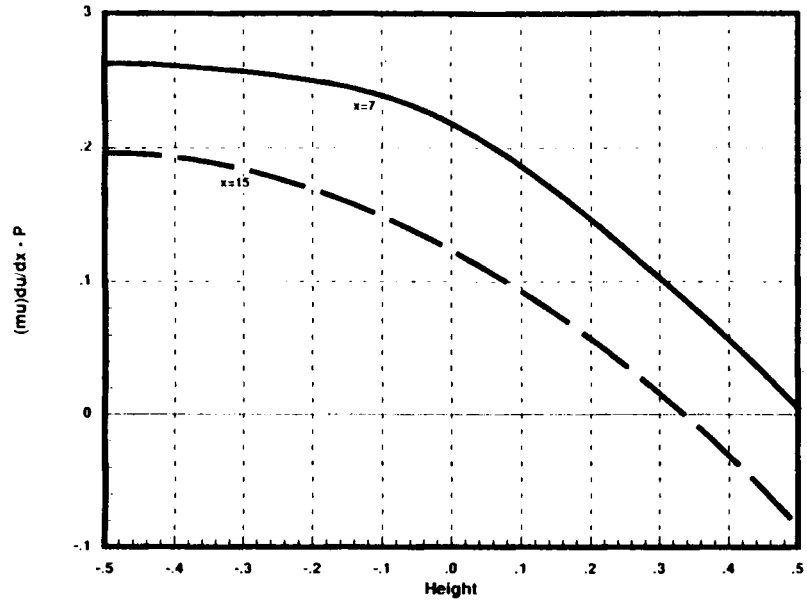

Figure 20. Vertical profiles of $(1/Re)\partial u/\partial x - P$ at $x = 7$ (solid line) and $x = 15$ (dashed line)

The nodal hydrostatic pressure was calculated from the simulation results at $x = 15$ and 7 via the formula

$$P_{i-1} = P_i + \frac{1}{Fr}\left(\frac{T_{i-1} + T_i}{2}\right)(y_{i-1} - y_i) \tag{10}$$

where P_{imax}, the pressure at the top node of the grid, was assumed to be zero and the integration proceeded downwards. The results of this calculation are presented in Figure 21. Also shown in Figure 21 is the difference between the simulation pressure and the hydrostatic pressure normalized by the pressure at the bottom at the grid. While the calculated pressure is within 1% of the hydrostatic at $x = 15$, there is a significant deviation (greater than 10%) from hydrostatic at $x = 7$ caused by the dynamic pressure of the eddy.

6. DISCUSSION

In an attempt to measure the accuracy of the results via a Richardson extrapolation, the simulation was repeated using grids with one-half and one-quarter of the original resolution, i.e. grids of 40×240 and 20×120. However, the 20×120 grid was too coarse to be within the convergence range and the results were inconclusive.

However, we felt that the 40×240 results were accurate enough and therefore performed a Richardson extrapolation assuming $O(h^2)$ error behaviour for the eddy statistics. Tables III and IV presents these results. On the basis of this, we believe that the results presented herein for the stratified backward-facing step as defined in Section 2 are within 1% of the correct solution.

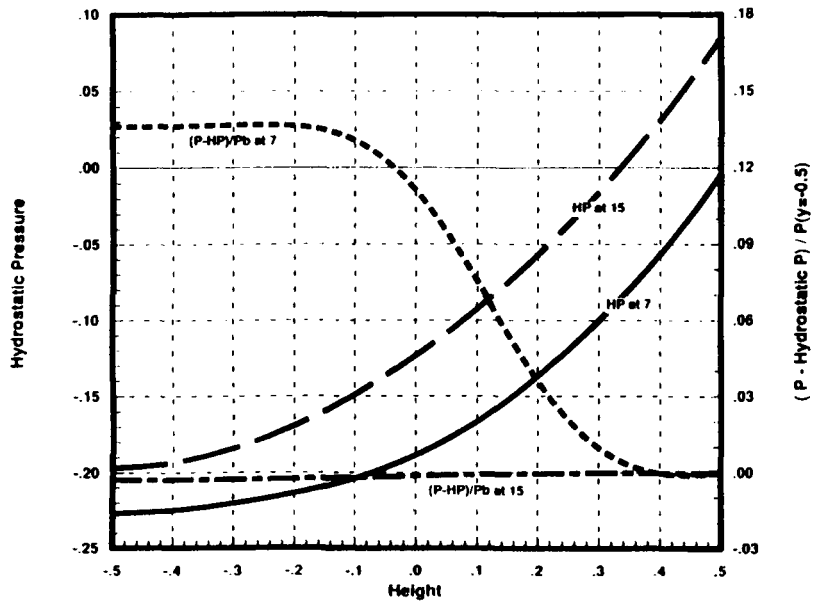

Figure 21. Vertical profiles of the hydrostatic pressure (HP) defined by equation (10) at $x = 7$ (solid line) and $x = 15$ (dashed line). Also, vertical profiles of the difference between the actual calculated pressure and the hydrostatic pressure normalized by the calculated bottom pressure for $x = 7$ (dotted line) and $x = 15$ (chain line)

Table III. Eddy positions and lengths resulting from $O(h^2)$ Richardson extrapolation using the 80 × 480 and 40 × 240 grid results

Eddy	Start x	Stop x	Length
1 (bottom)	0·000	0·355	0·355
2 (bottom)	0·355	2·508	2·153
3 (bottom)	4·565	8·413	3·848
4 (top)	1·215	5·512	4·297
5 (top)	8·188	10·234	2·046

Table IV. Eddy streamfunction (extremum minus separation) values and positions resulting from $O(h^2)$ Richardson extrapolation using the 80 × 480 and 40 × 240grid results

Eddy	Extremum value	x-co-ordinate	y-co-ordinate
1 (bottom)	0.00008	0·0125	−0·4000
2 (bottom)	−0.02241	1·500	−0·2583
3 (bottom)	−0.00852	6·625	−0·3000
4 (top)	0.01880	4·042	0·2417
5 (top)	0.00017	9·208	0·4500

ACKNOWLEDGEMENTS

The author would like to acknowledge the contributions of Dr. P. M. Gresho and Dr. S. T. Chan, who developed many of the algorithms used in the model employed here and who participated in many helpful discussions. The author would also like to thank Marilyn Borton for typing the manuscript.

This work was performed under the auspices of the U.S. Department of Energy by the Lawrence Livermore National Laboratory under contract W-7405-ENG-48.

REFERENCES

1. P. M. Gresho and S. T. Chan, 'A semi-implicit method for solving the time-dependent conservation equations for incompressible flow', *Numerical Methods in Laminar and Turbulent flow, Part 1*, Pineridge Press, Swansea, 1985, pp. 3–21.
2. W. Sun, 'A forward–backward time integration scheme to treat internal gravity waves', *Mon. Weather Rev.*, **108**, 402–407 (1980).
3. J. M. Leone Jr., P. M. Gresho, R. L. Lee and R. L. Sani, 'Flow-through boundary conditions for time-dependent, buoyancy-influenced flow simultions using low order finite elements', *Numerical methods in Laminar and Turbulent Flow*, Pineridge Press, Swansea, 1983, pp. 3–13.